Available online at www.sciencedirect.com
ScienceDirect
Journal of Solid State Chemistry 179 (2006) 3784–3797
JOURNAL OF SOLID STATE CHEMISTRY
www.elsevier.com/locate/jssc

Microwave-treated layered double hydroxides containing Ni^{2+} and Al^{3+}: The effect of added Zn^{2+}

P. Benito, F.M. Labajos, V. Rives*

Departamento de Química Inorgánica, Universidad de Salamanca, Salamanca-37008, Spain

Received 20 June 2006; received in revised form 10 August 2006; accepted 12 August 2006
Available online 17 August 2006

Abstract

Ni containing layered double hydroxides (LDHs) have been prepared by precipitation and hydrothermally treated under microwave irradiation for different periods of time. The solids have been calcined at three temperatures corresponding to stable phases formed during thermal decomposition of LDHs. The properties of the irradiated samples and of the calcined products were studied in order to ascertain whether the ageing treatment under microwave irradiation modifies not only the properties of the layered materials, but also the properties of the calcined products. A structural and textural study was carried out by PXRD, FT-IR and Vis–UV spectroscopy, thermal analyses (DTA and TG), N_2 adsorption/desorption at −196 °C and TEM microscopy; the reducibility of the nickel species was studied as well by TPR. The results show that the microwave treatment leads to better crystallized LDHs with modified thermal stability and reducibility. In addition, the degree of crystallinity of the layered precursors and their textural properties determine the properties of their thermal decomposition products.
© 2006 Elsevier Inc. All rights reserved.

Keywords: Hydrotalcite; Nickel; Zinc; Microwave; Hydrothermal; Reducibility; Calcinations

1. Introduction

Layered double hydroxides (LDHs) or hydrotalcite-like compounds (HTlc) are layered materials with the brucite-like structure where a partial substitution of the divalent cations has taken place; anions (and water molecules) are located in the interlayer region balancing the charge excess [1–3]. A wide variety of materials have been prepared modifying both the layer and interlayer species. Much of the research carried out on this kind of materials has been a consequence of the wide and different applications in catalysis as such [4–6], and also because calcination of HTlcs leads to a homogeneous mixture of basic oxides with very small crystallite size, stable against thermal treatments and able to yield small and thermally stable metal crystallites by reduction. All these features are a consequence of the homogeneous distribution of the cations within the brucite-like sheets.

Among all the HTlcs synthesized, those containing nickel cations in the layers have been and are still widely used as catalysts [5] because of the low cost of nickel, together with the advantages previously reported for the oxides obtained after thermal treatments. For instance, they have been successfully applied for partial oxidation, steam, dry and autothermal reforming of methane where severe reaction conditions are required [3,6] as an alternative to supported noble metals, decreasing coke formation and subsequent catalyst deactivation. The reducibility of Ni^{2+} cations existing in the LDH is a crucial parameter in some processes, for example, in determining the steam reforming activity [7]. Furthermore, the activity of these catalysts has been also related to their acid–base and/or redox properties, which in turn depend on their composition (i.e., the nature and molar fraction of cations in the layers), the preparation method and the treatment to which they have been submitted [8]. As mentioned, some catalytic processes are also carried out over as-synthesized Ni-HTlcs, that is, not thermally activated HTlcs, for instance, migration of the double

*Corresponding author. Fax: +34 923 29 45 74.
E-mail address: vrives@usal.es (V. Rives).

0022-4596/$ - see front matter © 2006 Elsevier Inc. All rights reserved.
doi:10.1016/j.jssc.2006.08.010

bond of eugenol to isoeugenol, for oxidation of allylic and benzylic alcohols and in Knoevenagel condensation [9–11], where the activity trends are correlated to the crystallinity of these materials and not to their specific surface areas (SSAs) and, in addition, the catalytic performance is considerably decreased upon calcination.

Other applications of the Ni-containing HTlc are based on their electrochemical properties [12]; Sugimoto et al. [13] studied the crystallinity dependence of the cell performance, showing that the crystallinity of the material also improved the electrochemical behaviour.

Another well-known property of the HTlc is the easiness with which a modification in their chemical composition affects some specific properties. For instance, inclusion of Zn in the structure modifies the electrochemical properties [14] and the catalytic performance [15,16] of Ni, Al LDHs. The results showed that the addition of zinc improved the electrochemical performance of the LDHs-based electrodes and that the zinc-modified catalysts produced smaller amounts of coke and methane during selective hydrogenation of acetylene.

The conventional and most widely used method to prepare nickel-containing hydrotalcites is by coprecipitation [17]. In order to obtain well-crystallized materials, coprecipitation has been coupled in some cases to hydrothermal treatment [18–20]. Recently, microwave radiation heating has been applied to the synthesis of LDHs with different chemical compositions as an alternative to the conventional hydrothermal treatments, showing several advantages such as shorter treatment times to achieve enhanced crystallinity degrees and higher SSAs [21–25]. Ni-containing materials have been also prepared by a microwave-assisted method [22,26].

In a previous paper [26] we have reported on the modification of the thermal properties and reducibility of nickel cations in as-synthesized LDHs. We here extend the study of the effect of hydrothermal treatment under microwave irradiation on the textural properties of the synthesized materials and on the nature and properties of the calcined products, paying special attention to the retention of the layered structure at low temperatures, and to the reducibility of the products calcined at moderate temperatures. In addition, zinc cations were included in the layer composition, comparing the results obtained in both series of samples. From this study, a relationship between the precursor properties and those of the calcined solids has been established.

2. Experimental

2.1. Synthesis of the solids

All chemicals were from Fluka (Switzerland) and the gases from L'Air Liquide (Spain), and were used without any further purification. The solids have been prepared by coprecipitation at constant pH: a solution, containing 0.25 mol of $Ni(NO_3)_2 \cdot 6H_2O$ and 0.125 mol of $Al(NO_3) \cdot 9H_2O$ dissolved in 500 mL of distilled water, was slowly added to a basic solution (NaOH and Na_2CO_3) with a slight excess (above the stoichiometric amount required to balance the positive charge in the layers due to the Al^{3+} cations) of carbonate to synthesize the Ni, Al-CO_3 samples, whereas for the preparation of the Zn, Ni, Al-CO_3 solids, 0.25 mol of $Ni(NO_3)_2 \cdot 6H_2O$, 0.25 mol of $Zn(NO_3)_2 \cdot 6H_2O$ and 0.250 mol of $Al(NO_3) \cdot 9H_2O$ were dissolved en 500 mL of distilled water to obtain the solution to be added to the carbonate solution. The pH was maintained constant at a value of 8.5 by continuous addition of a 1 M NaOH basic solution. The nominal M^{2+}/Al^{3+} molar ratio was 2/1, and for the zinc containing samples the nominal Zn^{2+}/Ni^{2+} ratio was 1/1. The slurry obtained was submitted to ageing treatments at 125 °C at autogenous pressure in a Milestone Ethos Plus multimode cavity microwave oven for different periods of time. The details of the procedure are described elsewhere [25]. The samples are named as follows: NA0 and ZNA0, for the non-aged Ni, Al and Zn, Ni, Al samples, respectively; NAHWt and ZNAHWt (where $t = 10$, 60, 180, 300 min stands for the treatment time), for the samples submitted to the microwave-hydrothermal treatment.

All the solids obtained were calcined at 225, 550 and 1000 °C in a static air atmosphere at a heating rate of 10 °C min^{-1}. The decomposition products were named adding −C1, −C2 and −C3 to the precursor names, corresponding to the solids calcined at 225, 550 and 1000 °C, respectively.

2.2. Characterization of the samples

Element chemical analyses for Ni, Al and Zn were carried out by atomic absorption in a Mark 2 ELL-240 apparatus, in Servicio General de Análisis Químico Aplicado (University of Salamanca, Spain). The powder X-ray diffraction (PXRD) patterns were recorded in a Siemens D-500 instrument using Cu$K\alpha$ radiation ($\lambda = 1.54050$ Å) and equipped with Diffrac AT software. Identification of the crystalline phases was made by comparison with the JCPDS files [27]. The FT-IR spectra were recorded in a Perkin-Elmer FT1730 instrument, using KBr pellets; 100 spectra (recorded with a nominal resolution of 4 cm^{-1}) were averaged to improve the signal-to-noise-ratio. The UV–Vis spectra were recorded following the diffuse reflectance (UV–Vis/DR) technique in a Perkin-Elmer Lambda 35 instrument with a Labsphere RSA-PE-20 integrating sphere and software UV WinLab, using 2 nm slits and MgO as reference. SSA assessment was carried out from the nitrogen adsorption–desorption isotherms at −196 °C recorded in a Gemini instrument from Micromeritics. The sample (ca. 80–100 mg) was previously degassed in flowing nitrogen at 110 °C for 2 h in a FlowPrep 060 apparatus, also from Micromeritics, in order to remove physisorbed water, and the data were analyzed using published software [28]. Thermogravimetric (TG) and differential thermal analyses (DTA) were carried out in TG-7 and DTA-7 instruments from Perkin-Elmer,

respectively, in flowing oxygen or nitrogen, at a heating rate of 10 °C min^{-1}. Temperature-programmed reduction (TPR) analysis was carried out in a Micromeritics 2900 TPD/TPR instrument; the reducing agent was H_2–Ar (5%vol) with a gas flow of 50 mL min^{-1}, the sample weight was 15–20 mg and the heating schedule 10 °C min^{-1} in order to avoid procedure artifacts [29]; calibration of the instrument was carried out with CuO (from Merck).

3. Results and discussion

3.1. LDHs

3.1.1. Chemical analyses

The M^{2+}/M^{3+} molar ratios for all samples are shown in Table 1. For the Ni, Al series a slight difference (ca. 10%) between the expected (2.0) and the experimental values (always larger than 2.0) is observed; this might be due to a preferential precipitation of one hydroxide or slight solubilization of Al^{3+} as aluminate. No significant difference in the M^{2+}/M^{3+} ratio is induced upon the microwave treatment, showing the stability of these materials under microwave irradiation. On the other hand, the measured values for the partially substituted Ni^{2+}/Zn^{2+} samples are closer to the expected ones, although a steady decrease in the Ni^{2+}/Zn^{2+} ratio (maximum difference 5%) is still observed as the microwave irradiation is prolonged. Similarly, the M^{2+}/M^{3+} ratio also decreases from the fresh sample to that irradiated for 300 min.

3.1.2. PXRD

The PXRD patterns for the Zn, Ni, Al series samples are included in Fig. 1. These patterns show the absence of secondary crystalline phases, such as ZnO—which is easily segregated when zinc-containing LDHs are submitted to hydrothermal treatments [30]—, are formed during the ageing process. The shape of the peaks is modified during the ageing treatment, pointing to structural and crystalline changes. The reflections become sharper and stronger when the slurry is submitted to longer microwave-hydrothermal treatments, a typical behaviour of better-crystallized materials. In addition, the doublet corresponding to planes (110) and (113) (recorded in the 2θ range 60–65°) also becomes better resolved, suggesting a better ordering of the cations in the layers. The crystallite size values were calculated from the broadening at half-height of the diffraction peaks due to planes (003) using the Debye–Scherrer method (Table 1). They confirm the enhancement in the ordering of the crystals in the basal direction. However, differences can be found in the crystallization process of both series, whereas as shown earlier, [26] microwave ageing has only a minor effect on the structural properties of Ni, Al-LDHs, in the Zn, Ni, Al samples here studied a more remarkable effect is observed; on one hand, it should be also born in mind that inclusion of zinc cations in the layers gives rise to better crystallized materials where the turbostratic disorder has almost disappeared [31]. On the other hand, the influence of the interaction of the electromagnetic radiation with the slurry cannot be neglected.

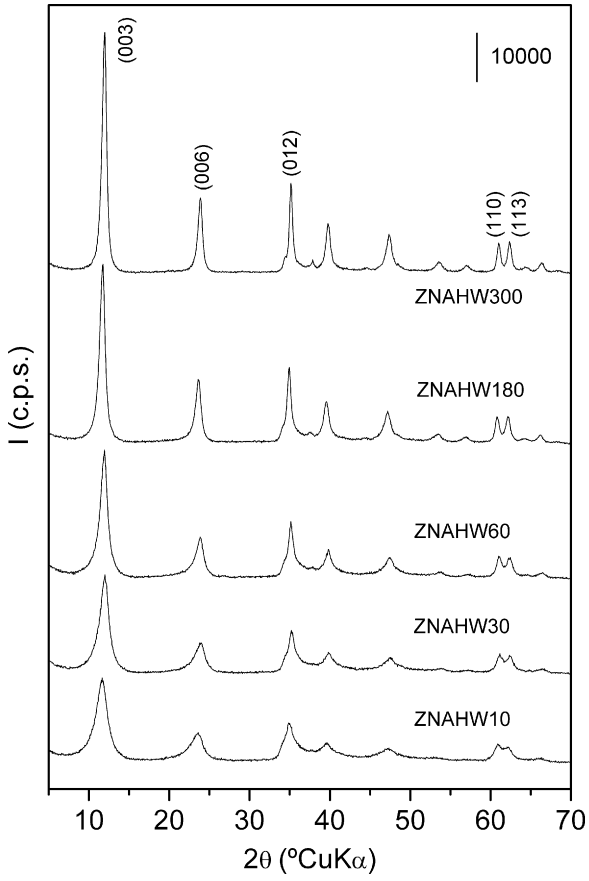

Fig. 1. PXRD patterns of the Zn, Ni, Al-CO_3 samples aged under microwave irradiation.

Table 1
Metal molar ratios (from element chemical analysis), lattice parameters (c and a, Å), crystallite size (D, Å), specific surface area (S_{BET}, $m^2 g^{-1}$) and H_2 consumption (experimental/calculated ratio) during TPR analyses for Ni, Al and Zn, Ni, Al samples

Sample	M^{2+}/M^{3+}	(Zn + Ni)/Al	c	a	D	S_{BET}	H_2
NA0	2.24		23.07	3.021	39	51	1.21
NAHW10	2.24		22.86	3.021	41	175	1.26
NAHW60	2.20		22.86	3.025	47	169	1.12
NAHW180	2.22		22.76	3.025	58	151	1.07
NAHW300	2.24		22.76	3.025	62	144	1.07
ZNA0	1.02	2.09	22.78	3.041	40	23	1.99
ZNAHW10	1.00	2.12	22.65	3.042	54	61	1.86
ZNAHW60	0.98	2.01	22.29	3.038	84	104	1.64
ZNAHW180	0.96	2.00	22.59	3.041	111	88	2.08
ZNAHW300	0.97	1.95	22.25	3.039	120	70	2.02

From the positions of lines due to reflexions by planes (110), (003) and (006), the cell parameters (Table 1) were calculated assuming an hexagonal cell, using the equations $a = 2d_{(110)}$, and $c = 3[1/2[d_{(003)} + 2d_{(006)}]$ [32]. Values for parameter a are almost constant, within experimental

error, for a given series of samples, 3.02 and 3.04 Å, for Ni, Al and Zn, Ni, Al series, respectively. This small difference arises from the larger size of Zn^{2+} than Ni^{2+} cations in an octahedral environment [33]. The *a* value does not change significantly for irradiated samples within a given series (with or without zinc), since no large variations in the layer composition exists. The *c* basal parameter roughly decreases slightly when the samples are aged under microwave radiation, suggesting stronger interactions between the layers and the interlayer anions [34].

The enhancement of the crystallinity of LDHs during hydrothermal treatment is believed to occur by Ostwald ripeining, a dissolution-precipitation process that leads to more crystalline and larger particles. This process can be fastened by the use of the electromagnetic radiation [25]. The microwave radiation uniformly and quickly heats all the solution avoiding thermal gradients. This heating is a consequence of the interaction of the radiation with the slurry. Water is the solvent, and, taking into account that it is a good microwave absorber, the microwave heating could be related to the dielectric heating of water; in addition, the possible formation of more active water molecules can help in the dissolution of the gel. However, LDHs can be also considered microwave absorbers, moreover, ionic conduction of the species located between the layers cannot be discarded, as it could be responsible for the improvement of the ordering in the interlamellar region as well. The differences observed between the two series of samples cannot be related to the different degrees of crystallinity of the coprecipitated samples, but it is necessary to consider that microwave interaction depends on the dielectric properties of the irradiated materials and, on modifying the layer composition, the dielectric properties could be changed as well [25].

3.1.3. FT-IR spectroscopy

The FT-IR spectra (those for the Zn, Ni, Al-CO_3 series are shown in Fig. 2) provide some additional clues about the crystallinity of the samples [25,34,35]. The broad band around 3400 cm^{-1} due to the ν_{OH} stretching mode of hydroxyl groups and water molecules is not significantly modified along the microwave treatment; however, the intensity and definition of the shoulder at ca. 2900 cm^{-1}, due to the stretching mode of OH groups hydrogen-bonded to interlayer carbonate anions [36], increases as the treatment time is prolonged, indicating stronger layer-interlayer interactions and a well ordered interlayer region also confirmed by the decrease of the *c* lattice parameter [34]. Further clues are given by the evolution of the $\nu_3(CO_3^{2-})$ band near 1400 cm^{-1} whose splitting reflects the decreased symmetry of the carbonate anions in the interlayer region. A decrease in the symmetry of this anion with respect to that for the free anion—D_{3h}—should exist in the fresh sample (ZNA0) because of the interaction of carbonate anions with water molecules; also the disordered species in the interlayer should account for the split band with two or three components. However, similarly to

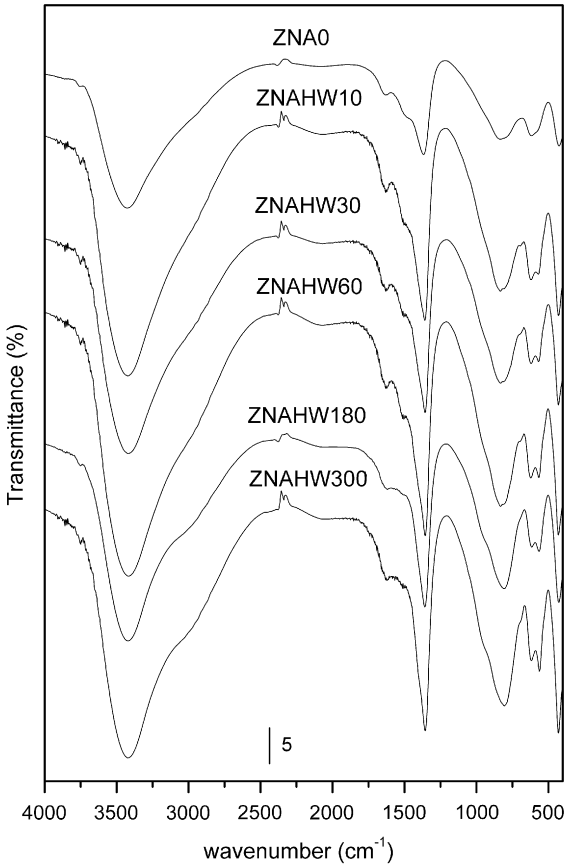

Fig. 2. FT-IR spectra of the Zn, Ni, Al-CO_3 samples.

samples treated under conventional hydrothermal treatment [34,35], the disorder in the interlayer space decreases when the irradiation treatment is prolonged, and the ν_3 band becomes sharper and more symmetric. In other words, the microwave treatment leads to an enhancement of the ordering of the interlayer species, due to the reorientation of water molecules and to the displacement of carbonate anions in response to microwave field; consequently, it is possible to achieve a better ordering of water molecules and carbonate anions in the interlayer space [25].

Regarding the low wavenumbers region, the intensity and sharpness of the bands in this range increases and, since the short-range structure around the metal cations does not change, as confirmed by the Vis–UV spectra (not shown), this points to a possible increase in the cation ordering within the layers [37,38].

3.1.4. TEM micrographs

Important differences have been found in the shape of the particles after the microwave treatment, Fig. 3. Only small and thin needle-like particles are observed for the fresh NA0 sample, but well-defined hexagonal platelets, characteristic of HTlc [39], develop after 60 min treatment. After coprecipitation, since nucleation and growth of the crystals take place simultaneously, a broad particle size distribution of small and thin needle-like particles is

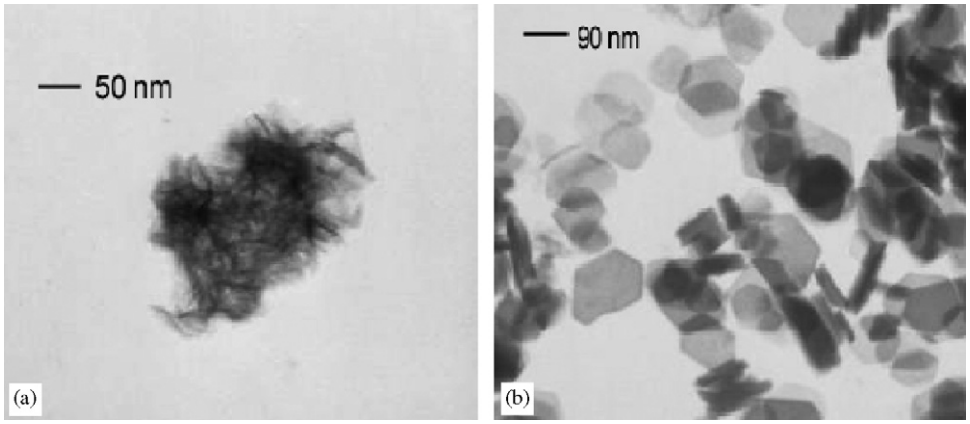

Fig. 3. TEM micrographs of Ni, Al samples: fresh sample, NA0 (a) and aged for 60 min under microwave-hydrothermal conditions, NAHW60 (b).

obtained. However, during the microwave hydrothermal treatment, the advantages of either hydrothermal conditions or microwave heating lead to hexagonal particles with uniform particle sizes. The small particles are dissolved and precipitate as larger particles giving rise to hexagonal particles. A further increase in the irradiation time leads to a decrease in the particle size, and a homogeneous particle size distribution of small particles is achieved. The TEM images for the Zn, Ni, Al samples show small particles with an uniform size and shapes similar to those here shown for the Ni, Al samples.

3.1.5. N_2 adsorption/desorption at −196 °C

The SSA values are included in Table 1. The increase in the SSAs, for the aged samples in comparison to those for the fresh ones, is typical of this kind of materials submitted to microwave-hydrothermal treatment. An important development of the SSA is first observed for samples treated for short periods of time, followed by a steady cancellation of the porosity as the exposure time to microwave irradiation is extended [21]. However, it should be remarked that although the PXRD analyses seem to point out that microwave-hydrothermal treatment (even for 10 min) has no appreciable effect on the structure of the materials, NAHW10 sample develops a very large SSA ($175\,m^2\,g^{-1}$), compared to the value ($50\,m^2\,g^{-1}$) for sample NA0; a similar increase percentage is observed for the Zn, Ni, Al samples. Probably this is a consequence of crystallization of mostly an amorphous (gelatinous) material in some sort of way blocking the pores. Changes in the porosity features result from an alteration of the microscopic morphology characteristics of the particles, since the mesoporous structure of LDHs may arise from interparticle space, as it was reported previously [25]. Crystalline samples usually are constituted by small particles, where the particle–particle interactions are very strong. Consequently, crystallite aggregation of face-to-face or card house type could account for the lower total external area values observed for the short time-treated samples. The increase observed in the SSAs upon microwave treatment can be related to the simultaneous nucleation of many nuclei, giving rise to small size particles with a higher (surface area/volume unit) ratio. In addition, the crystallinity enhancement leads to a lower probability of aggregates formation. However, when particles grow because of the dissolution-precipitation process (Ostwald ripening), the particle size increase becomes important, resulting in larger and well-formed crystals, so the (surface area/volume unit) ratio decreases [25]. These features agree with the results obtained by TEM microscopy.

All the N_2 adsorption–desorption isotherms recorded belong to type II in the IUPAC classification [40], with a H3 hysteresis loop, Fig. 4, but small changes in the shape of the hysteresis loop are observed. At a first sight, the modifications are quite similar to those previously reported [25], the hysteresis loop broadening for samples treated under the microwave field for short periods of time, and a progressive narrowing of the hysteresis loop for the Zn, Ni, Al compounds as the ageing treatment is prolonged. However, an anomalous behaviour is observed for the Ni, Al series: an irregular and broad loop develops in the sample irradiated for 10 min, where the adsorption and desorption branches are not parallel, but only after 180 min of microwave treatment the branches become parallel. The shape of the hysteresis loops has often been interpreted in terms of the specific pore structure, although it can be affected by other factors, such as the shape and lack of homogeneity in the size of the pores. In general terms, a significant difference in the relative pressures and slopes of the two branches of the hysteresis loops is usually taken as an indication of a heterogeneous pore geometry. On the contrary, a narrow hysteresis loop, with almost parallel adsorption and desorption branches, evidences a regular pore geometry, while a step desorption behaviour indicates that the pore sizes are in a narrow pore range. The broadening of the hysteresis loop for the NAHW10 sample can be also explained by either the dissolution of the amorphous particles emptying the pores, so leading to adsorption on larger radii pores. Then, the changes can be related to a progressive cancellation of interparticle pores because of the formation of larger particles.

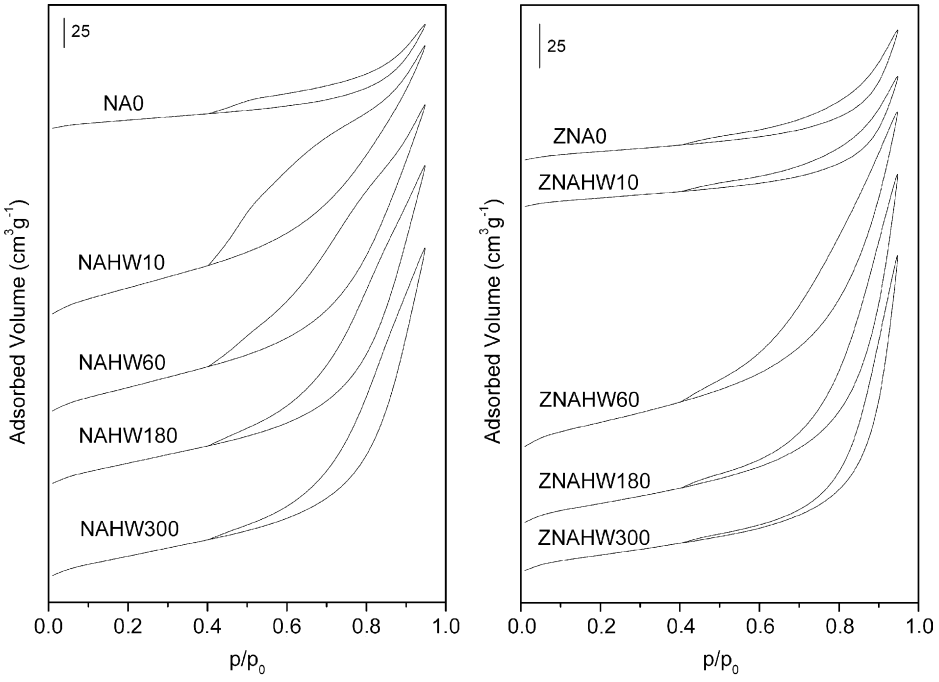

Fig. 4. N_2 adsorption isotherms for the Ni, Al-CO_3 and Zn, Ni, Al-CO_3 samples.

The pore size distributions were determined by the BJH method [41], and the results are shown in Fig. 5. A narrow peak centred at ca. 4 nm is observed for the fresh samples in both series, NA0 and ZNA0. Some changes in the shape of the distribution curve are observed for the microwave-treated solids. A shoulder at large pore radius develops and a wide contribution by pores in the 3–12 nm range is observed for the samples aged under microwave radiation, with a simultaneous decrease in the intensity of the main peak at ca. 4 nm. Both series differ in the relative contribution to the surface area by pores with large or small radii: whereas samples NAHW180 and NAHW300 show a high contribution to the surface area by large pores, the contribution by smaller pores becomes more relevant for the samples containing zinc aged for the same periods of time.

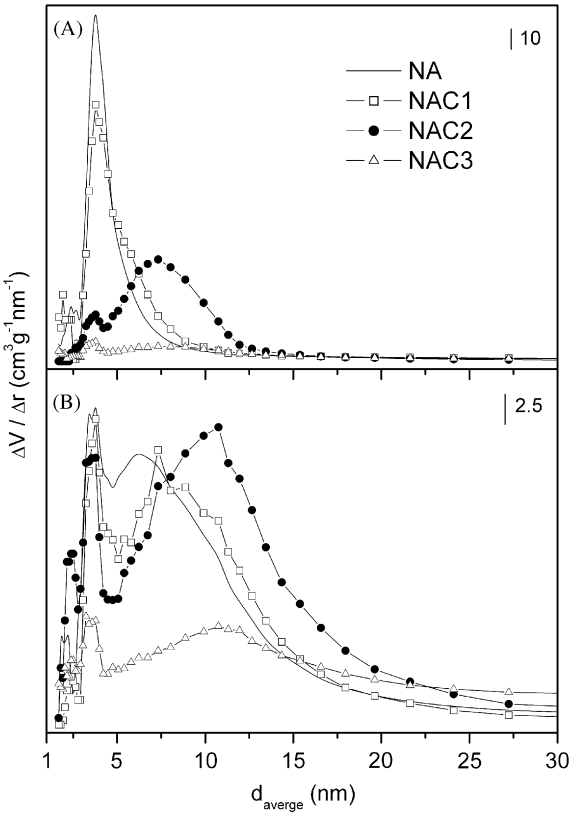

Fig. 5. BJH pore size distributions for fresh sample and samples aged for 10, 60, 180 and 300 min under microwave irradiation of Ni, Al and Zn, Ni, Al series.

3.1.6. Thermal analyses

In order to evaluate more accurately the effect of the microwave radiation on the thermal stability, the differential thermogravimetric curves (DTG) are included in Fig. 6. These curves provide a clearer view of the thermal effects than the integral TG curves, and the peaks are recorded in positions for which the DTA usually show the corresponding endothermic effects associated to the weight losses. The ageing treatment modifies the thermal behaviour of the samples because of an enhancement in the crystallinity degree. However, although the ageing treatment seems to have a remarkable influence on the crystallinity degree of zinc-containing samples (as concluded from the PXRD results), the thermal analyses evidence an important modification of the thermal properties of Zn-free samples too. We have previously shown [26] that water release from the interlayer space of Ni, Al LDHs takes place at higher temperatures for those samples treated under microwave radiation than for the untreated or conventionally aged

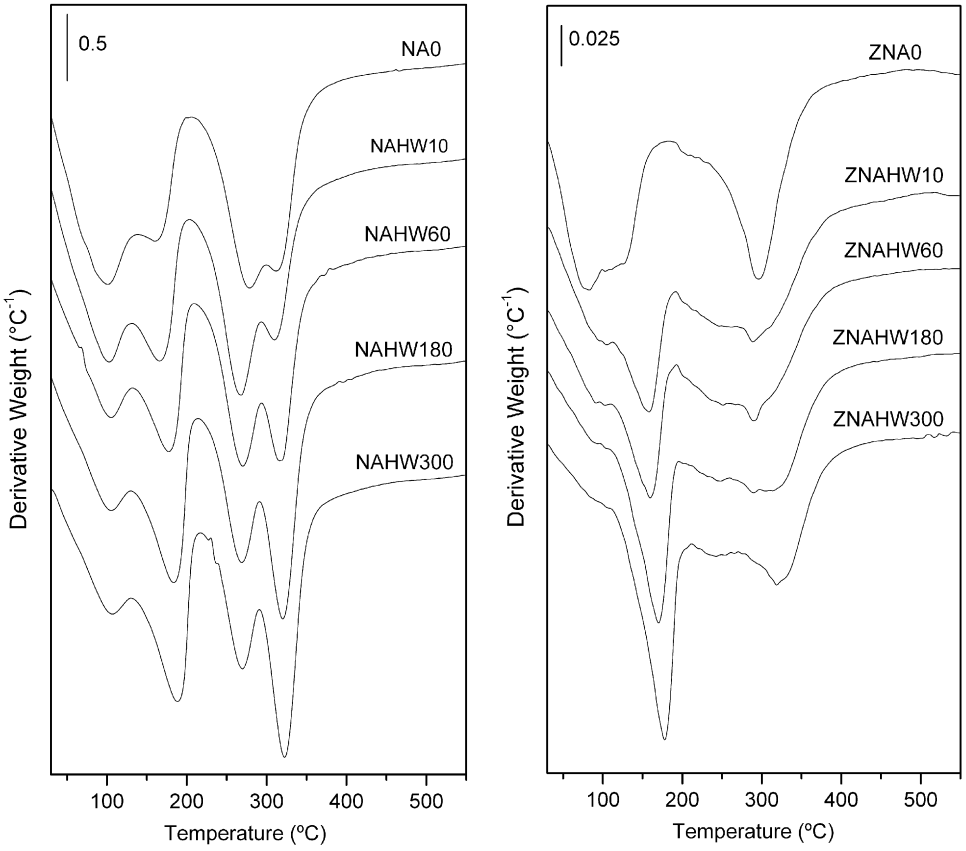

Fig. 6. DTG curves for Ni, Al and Zn, Ni, Al series recorded in oxygen.

ones. The endothermic decarbonation and dehydroxilation processes (usually recorded as a single peak in the DTA traces) split after the ageing process; on increasing the irradiation time the high-temperature effect is enhanced while the low-temperature one becomes weaker. These two facts are related to an enhancement of the crystallinity degree, leading to a better defined structure [7,21,22,26]. If this change in the thermal stability is related to a better ordered structure, the effect would be more intense for samples of the Zn, Ni, Al-CO_3 series than for samples Ni,Al-CO_3; however, such an effect is not always observed. The amount of physisorbed water (corresponding to the first weight loss) decreases considerably after a few minutes of microwave treatment for the Zn, Ni, Al samples. The evolution of the second weight loss is different: whereas sample ZNA0 shows a rather symmetric and intense DTG peak, it is broadened and extends in a wider temperature range for the microwave-treated samples. The DTA curves of these samples (not shown) show an additional effect around 800 °C. Although peaks in this range have been previously reported [42] and attributed to removal of residual carbonate anions, no weight loss is observed in this case, and thus it should be originated by crystallization of a spinel phase [43], which presence in the high temperature calcined solids has been evidenced by PXRD (see below).

The temperatures at which thermally stable phases are formed can be concluded from the thermal analyses. The hydrotalcite-like samples were calcined at three different temperatures, immediately after the main decomposition processes observed in the DTA and TG curves, namely, 225, 550 and 1000 °C, in order to study the possible effect of the microwave radiation on the properties of the products thus formed. Previous results have shown that the hydrothermal treatment has no influence on the thermal properties and crystallite sizes of the oxidic forms of the materials [34,44].

3.2. Calcined products

3.2.1. PXRD

The diffraction patterns of solids of the samples calcined at 250 °C (that is, once release of interlayer water has been completed) are shown in Fig. 7. The lamellar structure is still evident for all samples, whichever the duration of the MW treatment, but the (003) diffraction peak shows a broadening and a shift to a value ca. 6.6 Å [45,46]; moreover, the diffraction lines ascribed to the non basal planes are also broadened and the (110) and (113) peaks are overlapped. The shift in the position of the (003) diffraction line is due to a "grafting" of the carbonate anions into the brucite-type layers [47]. In addition, the broadening of the diffraction lines points that the structure becomes partially disordered; in other words, removal of interlayer water leads to destabilization of the

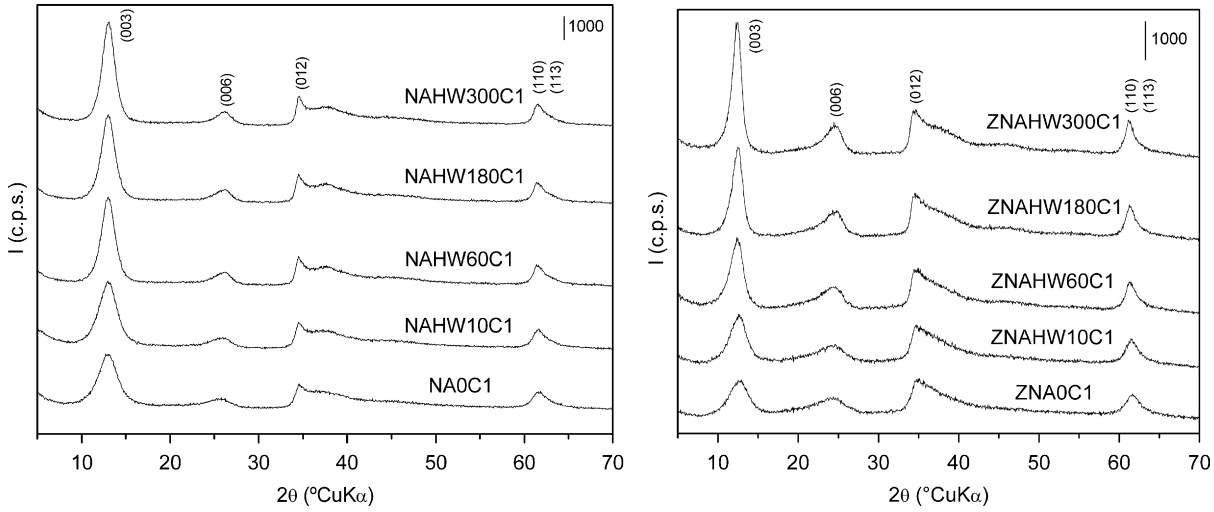

Fig. 7. PXRD patterns of the two series calcined at 225 °C: NAC1 (left) and ZNAC1 (right).

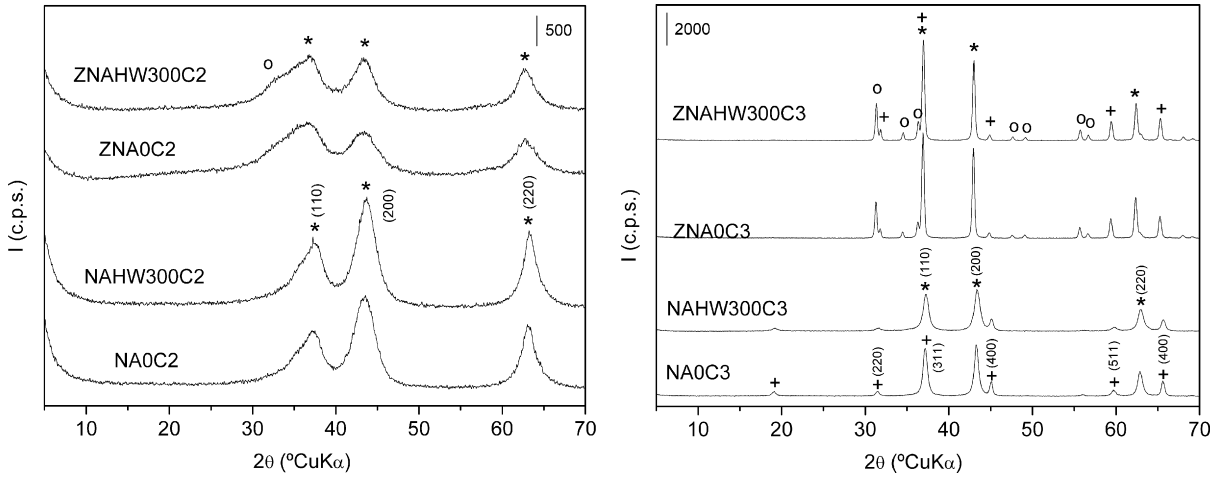

Fig. 8. PXRD patterns of the fresh and microwave-irradiated for 300 min samples of the Ni, Al and Zn, Ni, Al series calcined at 550 °C (left) and at 1000 °C (right). Legend: (*) NiO; (○) ZnO; (+) spinel phase ($NiAl_2O_4$ for NA compounds and $NiAl_2O_4$ or $ZnAl_2O_4$ for ZNA compounds).

hydrotalcite-type structure [48,49]. From the results here reported, we can conclude that retention of the original lamellar structure of the solids mainly depends on two factors: the nature of the cations located within the layers and the ageing to which the parent LDHs were submitted to. On comparing the PXRD patterns of the solids according to the post-treatment given, it should be noticed that the retention of the structural integrity of the HT-type lattice is determined by the crystallinity of the LDH precursor. The greater ability to retain the structural integrity of the more crystalline precursors may be very useful for applications of these materials under moderate temperatures [9–11], where the crystallinity order of the materials is more important than the SSA. Regarding the effect of the chemical composition, only minor differences are observed between the precursors and the dehydrated solids, although samples of the ZNA system show the greatest loss in the crystallinity degree.

On raising the calcination temperature to 500 °C, carbonate release and layer dehydroxylation have already taken place. At this step, the lamellar structure is destroyed and the PXRD diagrams show the presence of mostly amorphous species, with broad diffraction maxima, Fig. 8. The diffraction lines for NAC2 solids correspond to those of a rock-salt NiO phase (ICDD 4-835 (NiO)). Three broad diffraction maxima are observed at ca. 2θ 35°, 43 and 63°, ascribed to (110), (200) and (220) planes, respectively. Although only three weak diffraction maxima are observed, studies on the nature of the different crystallographic phases and on the reducibility of nickel as a function of takovite (a natural nickel–aluminum–carbonate hydrotalcite-type compound) composition led to propose a three phases model for the calcined solids: a NiO phase probably containing Al^{3+} impurities, a spinel-type phase located on the surface of NiO, and a nickel-doped Al_2O_3 phase possibly graphed on NiO and/or spinel phase. In other words, the NiO crystallites can be viewed as an oxide phase decorated by a spinel-type phase [44]. On the other hand, for the zinc-containing solids the maxima at ca. $2\theta = 42°$ and 62° correspond to NiO and the change

in the relative intensities of the peaks recorded close to 2θ 37° and 43° is due to the simultaneous presence of ZnO, whose diffraction maxima should be included in the broad tails of the main peaks of NiO [15].

No important differences are observed between the diffraction diagrams of the mixed oxides, probably because of the poor crystallinity of the phases. In an attempt of studying whether the microwave treatment has any effect in the crystallite size of the solids, an estimation of this parameter was made for samples of the NAC2 series, from the values of the full-width at half-maximum (FWHM) of the (220) diffraction peaks, Table 2. Values around 46–55 and 32–41 Å are measured for calcined NAC2 and ZNAC2 samples, respectively. From these values, it can be concluded that the post-treatment has no effect on the crystal size of the mixed oxides obtained by calcinations at 500 °C [50].

Although some differences are found between the values calculated for the lattice parameter of the calcined products derived from the samples aged under different conditions, they do not seem to follow any defined trend, Table 2. Because of the poor resolution of the diffraction diagrams, the changes observed might be related to a not well fitting of the peak position. Due to formation of a mixed oxide phase, the values for lattice parameter a are also smaller than that for the pure oxide (NiO, 4.177 Å, ICDD 4-835) [44]. Finally, the values calculated for NiO for the zinc-containing oxides are closer to that of the pristine NiO phase.

Calcination at high temperatures, 1000 °C, leads to phase segregation, Fig. 8. New and strong peaks located at 30.2°, 35.6°, 46°, 57.1° and 62.7° are recorded, assigned to the (220), (311), (400), (511) and (440) reflections of spinel-like structures. In addition, since the segregation of the spinel phase leads to the rearrangement of the atoms inside the rock-salt type phase, the oxide phases are less defective and their lattice parameters are close to the reported ones, Table 2. As for the mixed oxides formed after calcinations at 500 °C, the lattice parameters are independent on the ageing treatment the LDH precursors had been submitted to. Diffraction lines of both NiO and $NiAl_2O_4$ phases are recorded for NA series. When zinc is incorporated into the structure the patterns show reflections due to ZnO and NiO, as well as spinel reflections which could be equally ascribed to $NiAl_2O_4$ and/or $ZnAl_2O_4$; however, it is not possible to identify which divalent cation is present in the crystalline lattice, since there is hardly any difference between the diffraction angles of the spinels corresponding to the different metal cations. It should be remarked that the calculated parameter for the NiO phase is ca. 4.20 Å, larger than the expected 4.17 Å.

Table 2
Lattice parameters and crystallite sizes for the phases identified in the PXRD diagrams of the Ni, Al and Zn, Ni, Al calcined samples

Sample	Rock-salt phase (NiO)				Spinel phase, 1000 °C	
	550 °C		1000 °C			
	c (Å)	D (Å)	c (Å)	D (Å)	c (Å)	D (Å)
NA0	4.155	55	4.170	168	8.044	203
NAHW10	4.153	46	4.169	147	8.044	185
NAHW60	4.172	48	4.170	148	8.044	169
NAHW180	4.164	53	4.170	148	8.044	150
NAHW300	4.153	50	4.170	140	8.044	145
ZNA0	4.172	37	4.200	447	8.044	438
ZNAHW10	4.186	32	4.208	402	8.107	367
ZNAHW60	4.190	40	4.200	384	8.070	439
ZNAHW180	4.174	38	4.200	419	8.070	417
ZNAHW300	4.177	41	4.205	333	8.070	416

Quite surprisingly the crystallinity degree of the materials is the inverse to that observed for the uncalcined precursors and the samples calcined at lower temperatures, Table 2. For the oxide phase it was calculated from the (220) diffraction peak, and for the spinel phase from its (220) reflection as well. The decomposition process is believed to take place topotactically, i.e., water vapour and carbon dioxide escape through the surface without extensive change in the crystal morphology or dealumination of the brucite-like sheets [51], and consequently the cations keep their original relative positions during the thermal process, accounting for the well-known high dispersion of the cations within the host. Although at high temperatures both stoichiometric oxide and spinel phases are segregated, it seems that the stability of the original precursors would determine the segregation process [52].

3.2.2. *DR/Vis–UV spectroscopy*

The spectra of samples NA and ZNA calcined at 250 °C (not shown) are similar, almost coincident to those of the precursors, suggesting that no modifications of the local environment of the nickel cations in the layers takes place during the dehydration step. When calcining at moderate temperatures, 500 °C, in the case of the nickel-containing samples, it should be noted the increase in absorption along all the spectral range recorded; moreover, an intense charge transfer band in the ultraviolet region is recorded, which can be related to the formation of non-stoichiometric oxides during the calcination process. Finally, a broad absorption in the 600–800 nm range, ascribed to Ni^{2+} species located in both octahedral and tetrahedral holes [53].

Despite the similarity of the spectra for samples NAC2 and ZNAC2 (i.e., calcined at 550 °C), when they are calcined at 1000 °C some differences develop, suggesting different environments for the nickel cations in both cases, Fig. 9. The same charge-transfer band as in the oxides calcined at 500 °C is observed in the spectra of samples NAC3. A band with several maxima is observed between 500 and 800 nm, which are attributed to nickel cations in both octahedral and tetrahedral environments. On the other hand, the spectra for ZNAC3 samples show only the bands due to octahedrally coordinated Ni^{2+} species. These results provide further support to the results outlined from the PXRD diagrams. The crystalline species observed for

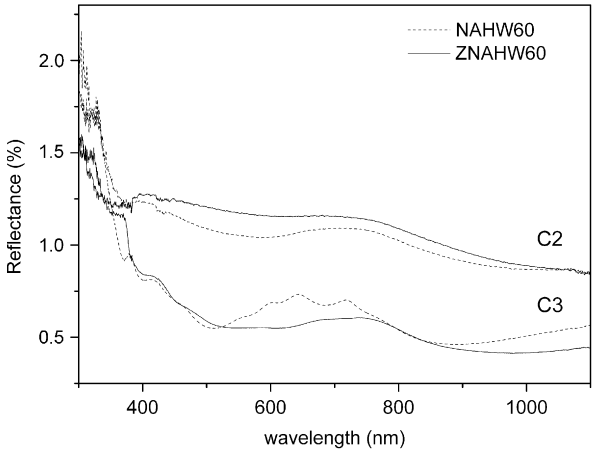

Fig. 9. DR/Vis–UV spectra for the samples calcined at 550 and 1000 °C of the NA and ZNA series.

the NAC3 samples are NiO and $NiAl_2O_4$, so the Ni^{2+} cations are in octahedral and tetrahedral holes, respectively. On the other hand, in the case of ZNAC3 samples the PXRD patterns did not permit to identify which spinel phase was segregated, $ZnAl_2O_4$ or $NiAl_2O_4$; taking into account the information obtained from the Vis–UV spectra it can be concluded that the only spinel phase is the zinc-aluminum one, since no bands due to tetrahedral species are observed in the spectra, and all bands were attributed to Ni^{2+} cations in an octahedral environment.

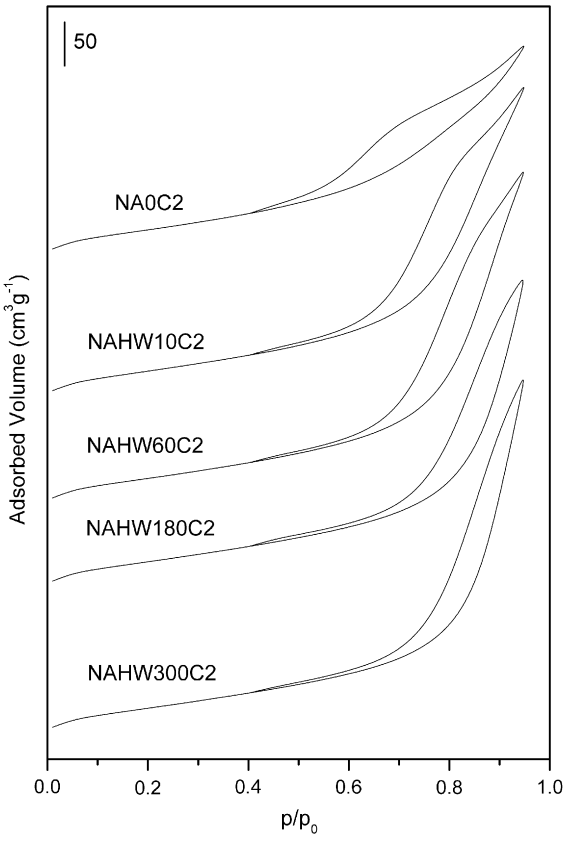

Fig. 10. N_2 isotherms of Ni, Al-CO_3 samples calcined at 550 °C.

3.2.3. N_2 adsorption/desorption at −196 °C

It is well established that calcination of LDHs gives rise not only to changes in their structure, but also to changes in their SSA and pore development. Reichle [54] reported that CO_2 and H_2O vapour evolution during thermal decomposition of carbonate-containing LDHs takes place through fines pores generated at the brucite-type layers, thus accounting for the increase in SSA observed in medium-temperature calcined samples. Because of the influence of the microwave-hydrothermal and conventional hydrothermal treatments on the textural properties of the LDH precursor, a comparative study of the evolution of the textural properties of the solids after being calcined at different temperatures was carried out.

The same kind of isotherm shape is recorded for most of the samples after the thermal treatments as for the as-synthesized samples. Minor changes are observed in the hysteresis loops, contrary to previous studies where the loop changes from type H3 for the uncalcined samples to H4 after calcination [55]. Solids heated at ca. 550 °C derived from LDHs with a low crystallinity degree develop broader hysteresis loops, while parallel adsorption/desorption branches are recorded for the oxides formed from better ordered compounds, Fig. 10. As commented above, the textural properties of the solids are determined by the particle morphology; in addition, the morphology of the solids is retained after the calcination process; as it is assumed that the decomposition process takes place topotactically, the textural properties of the calcined solids will be intimately related to those of the starting LDH precursors. Consequently, it is possible to control the textural properties of the precursors by applying microwave heating, and thereof it is possible to prepare materials with tailored textural properties. However, it should be remarked that the features are also observed in the solids calcined at 1000 °C, where a structural arrangement has taken place.

Fig. 11 shows the change in the BET specific surface areas (SSAs) against the ageing treatment for some representative precursors and samples calcined at different temperatures. In general terms, the evolution of the specific surface area is the same as that formerly reported for calcined hydrotalcite-like materials [54]. However, some aspects must be taken into account for the two series here studied. When calcining at 225 °C, the SSA remains almost constant for Ni, Al samples, being only larger in the case of the conventionally aged solids. Finally, when the nickel cations have been partially replaced by zinc ones all the solids undergo a surface development, of the same order for all the samples studied. Since very close SSAs are measured for samples calcined at 225 °C (a treatment leading only to dehydration of the interlayer space), the cratering mechanism proposed by Reichle should correspond only to escaping of water generated during collapsing of the layered structure through condensation of hydroxyl groups. Changes in the S_{BET} area values are also

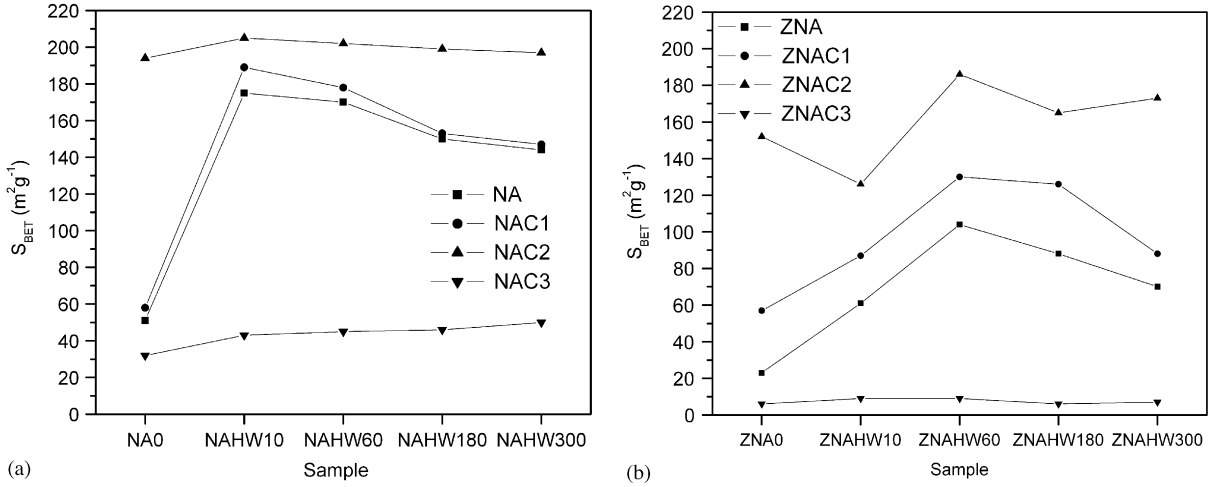

Fig. 11. S_{BET} evolution during thermal treatment of series Ni, Al-CO_3 (a) and Zn, Ni, Al-CO_3 (b).

consistent with the PXRD patterns, i.e., with the crystallinity degree of the dehydrated solids. The series for which the SSAs of the calcined samples are close to those of the precursors are the same for which the higher crystallinity degree is retained; this is the behaviour observed for the Ni, Al series, where the solids keep roughly the original structure, while for the Zn, Ni, Al series, where the solids are largely affected by heating at 225 °C, a larger surface development is observed.

On the other hand, despite the great differences in SSA values measured for the precursors, quite close values are obtained for the solids calcined at 550 °C. The SSA development is larger for those precursors with smaller areas, a behaviour typical of LDHs decomposition following a cratering mechanism [54], and of the presence of an aluminium oxide phase [44]. Mixed nickel oxides exhibit fairly similar SSAs, indicating that ageing has no large influence on the BET area of the mixed oxide, in good agreement with the crystal size values of the precursors, which remain roughly constant whichever the irradiation time. Finally, a random change in surface development is observed for samples ZNAC2.

On raising the calcination temperature up to 1000 °C the surface area available for nitrogen adsorption is drastically reduced for samples ZNAC3. The low N_2 adsorption capacity of this series of samples can be explained by the complete segregation of well crystallized oxide and spinel phases, in full agreement with the PXRD patterns. On the other hand, the samples derived from the other two series show high SSAs despite the high calcination temperatures, because of the higher stability against sintering of NiAlO binary oxides under heat treatment.

The pore size distribution curves of the calcined samples are included in Fig. 12. The changes observed in the BJH plots are in agreement with the changes observed in the shapes of the isotherms and the values of the SSAs. Similar pore size distribution curves are observed for original series Ni, Al samples and for those calcined at 225 °C, i.e., after release of interlayer water molecules. However, a broad pore size distribution is observed for the oxides formed at higher calcination temperatures, in agreement with a cratering mechanism. It should be noticed that the main changes in the pore size distributions are found for the calcined solids coming from the precursors aged for short periods of time, whereas the oxides obtained from the more crystalline LDHs do not show significant changes in their BJH plots. The bimodal pore size distribution is even observed for those solids where segregation of NiO and $NiAl_2O_4$ has taken place. Samples containing zinc do not follow the same trends, and no remarkable differences are found among their BJH plots after submitting them to calcination treatments. Such differences between series Ni, Al and Zn, Ni, Al can be related to the segregation of ZnO as as separate phase even at moderate calcinations temperatures.

3.2.4. TPR

Finally, the reducibility of the nickel cations in both the precursors and in the calcined solids has been also studied, Fig. 13. Differences can be found between the TPR profiles of samples aged for different periods of time. This finding is not unexpected, as the reduction process is carried out dynamically at increasing temperatures, and so the small differences observed in the TPR profiles might be related to the different decomposition behaviour; decomposition in H_2 should occur following steps similar to those occurring during calcination in air, at rather similar temperatures [56]. As shown in Fig. 13, the more remarkable differences are found in the Zn, Ni, Al series; however, as the thermal stability in air for these samples is only slightly modified after microwave treatment, different factors may be responsible for the behaviour observed in hydrogen.

On one hand, it is well-known that the low reducibility of Ni^{2+} ions in Ni, Al LDHs is due to the formation of a spinel-type phase decorating the NiO particles formed upon thermal decomposition of the LDHs; this spinel phase denies the access of the reducing gas to the surface [44,57]. Reduction of Ni^{2+} to Ni^0 in our samples the takes

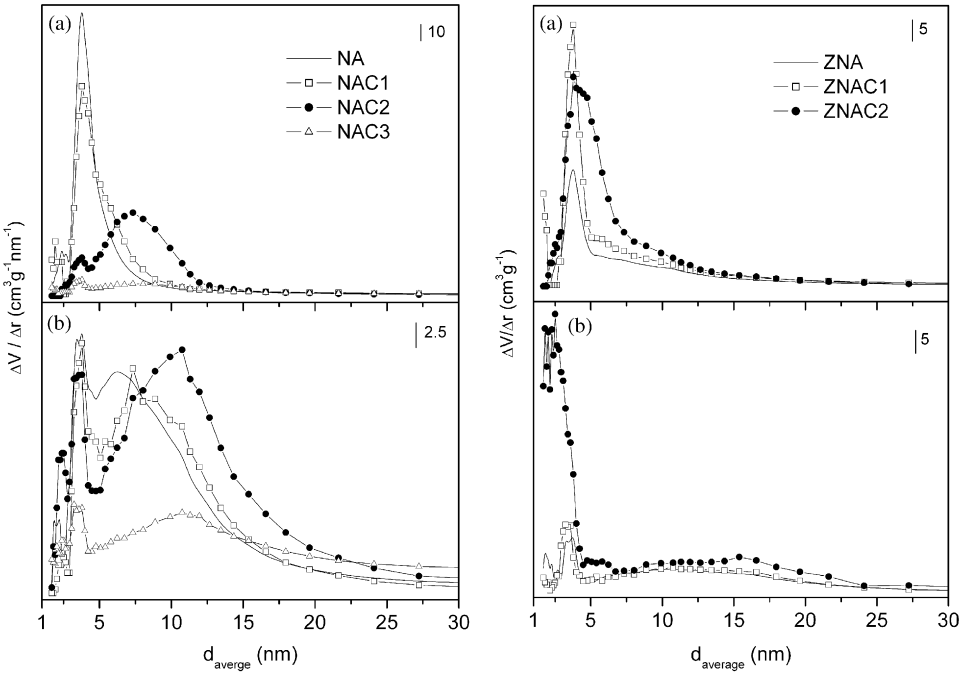

Fig. 12. BJH pore size distributions for calcined Ni, Al and Zn, Ni, Al series samples aged for 10 and 300 min.

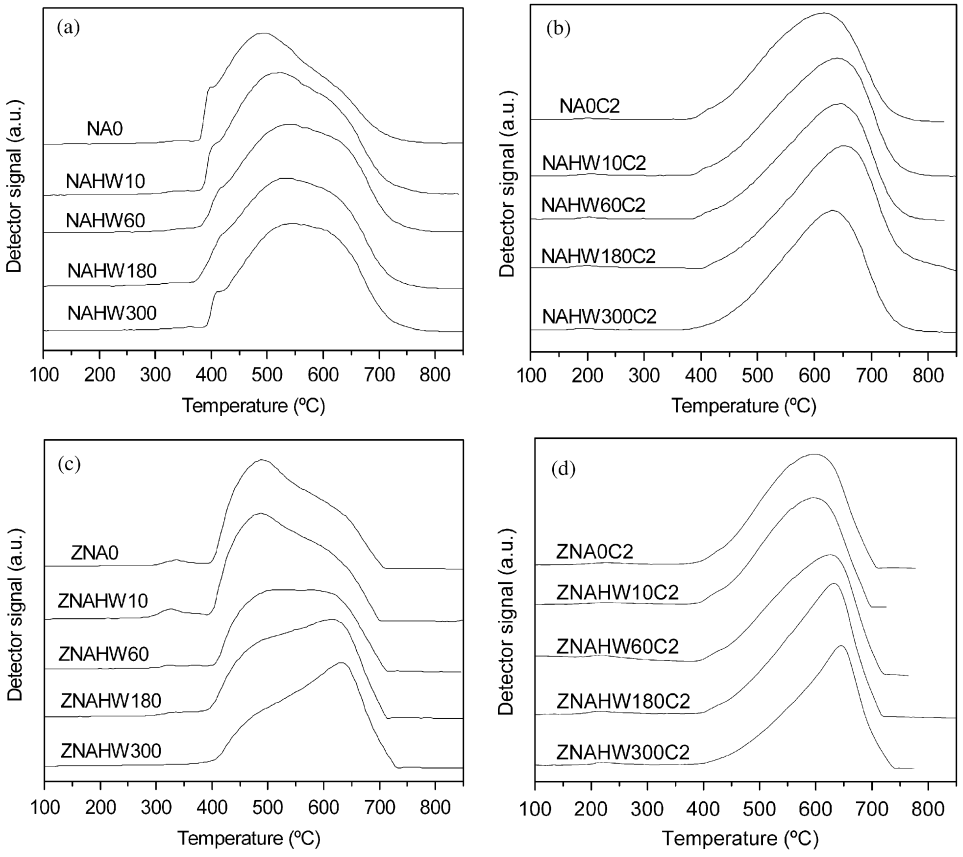

Fig. 13. TPR curves for the LDH precursors and calcined samples at 550 °C for the NA series (a, b) and ZNA series (c, d).

place in the 400–750 °C range, and it is characteristic of Ni^{2+} interacting with other elements [58,59]. The curves suggest the presence of two types of Ni^{2+}, probably free NiO responsible for the shoulder at low temperatures [9] and spinel-decorated NiO particles, accounting for the reduction maximum recorded at higher temperatures

[44,57]. Increasing the irradiation time leads to a steady shift of the maxima towards higher temperatures, a behaviour which might be related to the formation of well dispersed smaller NiO particles, with larger interface development, so being able to be more heavily decorated with the spinel phase, or supported on a nickel aluminate-type phase, making their reduction more difficult, as previously observed for other Ni,Al compounds [60]. The reduction maxima in the TPR profiles of the calcined samples are shifted towards high temperatures in comparison to the precursors; furthermore, the small reduction peak at low temperatures is much weaker than for the uncalcined precursors and it completely disappears for the calcined sample prepared from the precursors aged for longer periods of time. The maximum is recorded above 600 °C for all the calcined samples, but a slight shift towards higher temperatures is observed as well. However, the profile reverts towards lower temperatures for the NAHW300C2 sample. We can conclude that the enhancement in the crystalline degree of the precursors due to microwave irradiation may modify the intimate structure of the solid solution formed after calcination at moderate temperatures, which affects the stability against reduction of Ni^{2+} species; the higher the crystallinity degree, the more stabilized the Ni^{2+} cations are against reduction and sintering by the matrix, thus requiring higher reduction temperatures and resulting in a better dispersion of the nickel particles [60]. This fact has been previously observed by Jitianu and col. for sol–gel synthesized samples [20].

The presence of zinc induces a change in the reduction profile. In these samples the amount of Ni^{2+} cations is lower than in those of the Ni, Al series, the thermal decomposition pathway is modified by the inclusion of Zn^{2+} in the layers and different crystalline structures are formed for both types of solids because of the easy segregation of ZnO at low temperatures, as it was shown by the X-ray diffraction. Although Zn^{2+} cations in pristine ZnO are not reduced by hydrogen to the metallic form, when zinc-containing LDHs are calcined under a reducing atmosphere, non-stoichiometric oxides with a large concentration of lattice defects are formed, which may easily favour the reduction process [61,62]. Zinc oxide particles act as a dispersing agent for the NiO particles, and the interaction of the reducible Ni^{2+} species with the support is different, depending on the presence or the absence of ZnO [13–16,63]. So, Ni^{2+} species are easily reduced in the less crystalline samples and an increase in the ageing time leads to a decrease in the reducibility of Ni^{2+}. However, the important differences observed in the TPR profiles of the precursors are not so remarkable in the oxides prepared by calcination; a shift towards higher temperatures is observed as the crystallinity of the precursor is enhanced.

The amount of hydrogen consumed was calculated from the areas of the peaks and related to the concentration of reducible cations, Table 1. Hydrogen consumption for Ni, Al samples is very close to that required for stoichiometric reduction of Ni^{2+} to Ni (H_2/Ni ratio of 1.0). However, it reaches values as high as 2 for Zn,Ni,Al samples; a similar overconsumption of H_2 has been previously reported [56] and it has been attributed to the reduction of a non-stoichiometric NiO_{1+x} phase and to the reduction of some balancing anions [56]. However, in the present work this behaviour should be related to the Zn^{2+} to Zn^0 reduction process taking place simultaneously.

4. Conclusions

The results show that the use of microwave radiation yields to a better order in the layer stacking the interlayer space and the cations within the hydroxide sheets; however, the extent of the improvement achieved is larger for the Zn, Ni, Al-CO_3 compounds. Furthermore, the thermal properties are intimately determined by the nature of the lamellar cations and the crystalline degree of the precursors. In this way, retention of the original lamellar structure by calcining at 225 °C is related to the crystallinity of the precursor; however, regarding the mixed oxides prepared by calcination at 550 °C no differences were found and finally the inverse crystalline order to that present in the precursors is observed for the phases segregated at 1000 °C. The TPR profiles of both the precursors and the calcined products have shown that the reducibility of the nickel species is also varied in relation to the LDH precursor. Finally, it is possible to control the textural properties of the precursors by applying the microwave heating and thereof it is possible to prepare materials with tailored textural properties.

Acknowledgments

Financial support from MCyT (grant MAT2003-06605-C02-01), ERDF and JCyL (grant SA030/03), and a grant from JCyL to PB are acknowledged.

Appendix A. Supplementary materials

Supplementary data associated with this article can be found in the online version at doi:10.1016/j.jssc.2006.08.010.

References

[1] V. Rives (Ed.), Layered Double Hydroxides: Present and Future, Nova Science Publishers, New York, 2001.
[2] F. Wypych, K.G. Satyanarayana (Eds.), Clay Surfaces: Fundamentals and Applications, Elsevier, Amsterdam, 2004.
[3] X. Duan, D.G. Evans, Structure and Bonding, Layered Double Hydroxides 119 (2006).
[4] F. Basile, A. Vaccari, in: V. Rives (Ed.), Layered Double Hydroxides: Present and Future, Nova Science Publishers, New York, 2001, p. 285.
[5] A. Monzon, E. Romeo, A.J. Marchi, in: V. Rives (Ed.), Layered Double Hydroxides: Present and Future, Nova Science Publishers, New York, 2001, p. 321.
[6] S. Albertazzi, F. Basile, A. Vaccari, in: F. Wypych, K.G. Satyanarayana (Eds.), Catalytic Properties of Layered Double

Hydroxides, Clay Surfaces: Fundamentals and Applications, Elsevier, Amsterdam, 2004, p. 497.
[7] S.R. Segal, K.B. Anderson, K.A. Carrado, C.L. Marshall, Appl. Cat. A: Gen. 231 (2002) 215–226.
[8] S. Casenave, H. Martinez, C. Guimon, A. Auroux, V. Hulea, A. Cordoneanu, E. Dumitriu, Thermochim. Acta 379 (2001) 85–93.
[9] B.M. Choudary, M.L. Kantam, A. Rahman, Ch.V. Reddy, K.K. Rao, Angew. Chem. Int. Ed. 40 (2001) 166–763.
[10] U. Costantino, M. Curini, F. Montanari, M. Nocchetti, O. Rosati, J. Molec. Catal. A: Chem. 195 (2003) 245–252.
[11] D. Kishore, S. Kannan, Appl. Catal. A: Gen. 270 (2004) 227–235.
[12] E. Scavetta, M. Berrettoni, M. Giorgetti, D. Tonelli, Electrochim. Acta 47 (2002) 2451–2461.
[13] A. Sugimoto, S. Ishida, K. Hanawa, J. Electrochem. Soc. 146 (1999) 1251–1255.
[14] H. Chen, J.M. Wang, T. Pan, H.M. Xiao, J.Q. Zhang, C.N. Cao, Int. J. Hydrogen Energy 27 (2002) 489–496.
[15] A. Monzón, E. Romeo, C. Royo, R. Trujillano, F.M. Labajos, V. Rives, Appl. Cat. A: Gen. 185 (1999) 53–63.
[16] J.C. Rodríguez, A.J. Marchi, A. Borgna, A. Monzón, J. Catal. 171 (1997) 268–278.
[17] F.M. Labajos, V. Rives, M.A. Ulibarri, Spectrosc. Lett. 24 (1991) 499–505.
[18] O. Clause, M. Gazzano, F. Trifirò, A. Vaccari, L. Zatorski, Appl. Catal. 73 (1991) 217–236.
[19] S. Kannan, A. Narayanan, C.S. Swamy, J. Mater. Sci. 31 (1996) 2353–2360.
[20] M. Jitianu, M. Balasoiu, R. Marchidan, M. Zaharescu, D. Crison, M. Criau, Int. J. Inorg. Mat. 2 (2000) 287–300.
[21] S. Kannan, R.V. Jasra, J. Mater. Chem. 10 (2000) 2311–2314.
[22] S. Möhmel, I. Kurzawski, D. Uecker, D. Müller, W. Gebner, Cryst. Res. Technol. 37 (2002) 359–369.
[23] D. Tichit, A. Rolland, F. Prinetto, G. Fetter, M.J. Martínez-Ortiz, M.A. Valenzuela, P. Bosch, J. Mater. Chem. 12 (2002) 3832–3838.
[24] M.J. Climent, A. Corma, S. Iborra, K. Epping, A. Velty J. Catal. 225 (2004) 316–326.
[25] P. Benito, F.M. Labajos, V. Rives, Microporous Mesoporous Mater. 94 (2006) 148–158.
[26] P. Benito, F.M. Labajos, V. Rives, Mater. Sci. Forum (2006) 514–516, 1284–1288.
[27] JCPDS: Joint Committee on Powder Diffraction Standards, International Centre for Diffraction Data, Swarthmore, PA, 1977.
[28] V. Rives, Adsorp. Sci. Technol. 8 (1991) 95–104.
[29] P. Malet, A. Caballero, J. Chem. Soc. Faraday Trans. I 84 (1988) 2369–2375.
[30] J.T. Kloprogge, L. Hickey, R.L. Frost, J. Solid State Chem. 177 (2004) 4047–4057.
[31] T.N. Ramesh, R.S. Jayashree, P.V. Kamath, Clays Clay Miner. 51 (2003) 570–576.
[32] F. Cavani, F. Trifirò, A. Vaccari, Catal. Today 11 (1991) 173–301.
[33] J.E. Huheey, E.A. Keiter, R.L. Keiter, in: Inorganic Chemistry. Principles of Structure and Reactivity, fourth ed, Harper Collins, New York, 1993.
[34] F.M. Labajos, V. Rives, M.A. Ulibarri, J. Mater. Sci. 27 (1992) 1546–1552.
[35] L. Hickey, J.T. Kloprogge, R.L. Frost, J. Mater. Sci. 35 (2000) 4347–4355.
[36] J.T. Kloprogge, R.L. Frost, in: V. Rives (Ed.), Layered Double Hydroxides: Present and Future, Nova Science Publishers, New York, 2001, p. 139.
[37] S. Velu, V. Ramkumar, A. Narayanan, C.S. Swamy, J. Mater. Sci. 32 (1997) 957–964.
[38] M.J. Hernández-Moreno, M.A. Ulibarri, J.L. Rendón, C.J. Serna, Phys. Chem. Miner. 12 (1985) 34–38.
[39] Z.P. Xu, P.S. Braterman, J. Mater. Chem. 13 (2003) 268–273.
[40] K.S.W. Sing, D.H. Everett, R.A.W. Haul, L. Moscou, R.A. Pierotti, J. Rouquerol, T. Siemieniewska, Pure Appl. Chem. 57 (1985) 603–619.
[41] E.P. Barret, L.G. Joyner, P.P. Halenda, J. Am. Chem. Soc. 73 (1951) 373–380.
[42] R.L. Frost, W.N. Martens, K.L. Erickson, J. Thermal Anal. Calorymetry 82 (2005) 603–608.
[43] A.H. Padmasri, A. Venugopal, V.D. Kumari, K.S.R. Rao, J. Molec. Catal. A: Chem. 188 (2002) 255–265.
[44] O. Clause, B. Rebours, E. Merlen, F. Trifirò, A. Vaccari, J. Catal. 133 (1992) 231–246.
[45] L. Pesic, S. Salipurovic, V. Markovic, D. Vucelic, W. Kagunya, W. Jones, J. Mater. Chem. 2 (1992) 1069–1073.
[46] F. Rey, V. Fornés, J.M. Rojo, J. Chem. Soc. Faraday Trans. 88 (1992) 2233–2238.
[47] Ts. Stanimirova, I. Vergilov, G. Kirov, N. Petrova, J. Mater. Sci. 34 (1999) 4153–4161.
[48] L. Chmielarz, P. Kutrowski, A. Rafalska-Łasocha, R. Dziembaj, Thermochim. Acta 395 (2003) 225–236.
[49] D. Tichit, M.N. Bennani, F. Figueras, J.R. Ruiz, Langmuir 14 (1998) 2086–2091.
[50] J. Sanchez Valente, F. Figueras, M. Gravelle, P. Kumbhar, J. Lopez, J.-P. Besse, J. Catal. 189 (2001) 370–381.
[51] Y. Seida, T. Nakano, Y. Nakamura, Water Res. 35 (2001) 2341–2346.
[52] M.A. Ulibarri, I. Pavlovic, C. Barriga, M.C. Hermosín, J. Cornejo, Appl. Clay Sci. 18 (2001) 17–27.
[53] A.B.P, Lever in Inorganic Electronic Spectroscopy, Elsevier, New York, 1984.
[54] W.T. Reichle, Solid State Ionics 22 (1986) 135–141.
[55] D. Tichit, F. Medina, B. Coq, R. Dutrarte, Appl. Cat. A: Gen. 159 (1997) 241–258.
[56] O. Levedeva, D. Tichit, B. Coq, Appl. Catal. A: Gen. 183 (1999) 61–71.
[57] F. Trifirò, A. Vaccari, O. Clause, Catal. Today 21 (1994) 185–195.
[58] B. Coq, D. Tichit, S. Ribet, J. Catal. 189 (2000) 117–128.
[59] G. Fornasari, M. Gazzano, D. Matteuzzi, F. Trifirò, Appl. Clay Sci. 10 (1995) 69–82.
[60] K. Schulze, W. Makowski, R. Chyzy, R. Dziembaj, G. Geismar, Appl. Clay Sci. 18 (2001) 59–69.
[61] R.J. Tilley, Deffect Crystal Chemistry and its Applications, Blackie, Glasgow/London, 1987.
[62] C. Barriga, F. Kooli, V. Rives, M.A. Ulibarri, Synthesis of Porous Materials (Zeolites, Clays and Nanostructures), in: M.L. Occeli, H. Kessler (Eds.), Marcel Dekker Inc., New York, p. 661.
[63] R. Unnikrishann, S. Narayanan, J. Molec. Cat. A: Chem. 144 (1999) 173–179.